Biophysical Characterization of Elongin C from *Saccharomyces cerevisiae*†

Alexander Buchberger,‡,§ Mark J. Howard,*,‡ Stefan M. V. Freund,‡ Mark Proctor,‡ P. Jonathan G. Butler,|| Alan R. Fersht,‡ and Mark Bycroft‡

MRC Centre for Protein Engineering, Department of Chemistry, University of Cambridge, Lensfield Road, Cambridge, CB2 1EW, U.K., and MRC Laboratory of Molecular Biology, Hills Road, Cambridge, CB2 2QH, U.K.

Received April 12, 2000; Revised Manuscript Received June 13, 2000

ABSTRACT: Elongin C (ELC) is an essential component of the mammalian CBC^{VHL} E3 ubiquitin ligase complex. As a step toward understanding the role of ELC in assembly and function of CBC-type ubiquitin ligases, we analyzed the quaternary structure and backbone dynamics of the highly homologous Elc1 protein from *Saccharomyces cerevisiae*. Analytical ultracentrifugation experiments in conjunction with size exclusion chromatography showed that Elc1 is a nonglobular monomer over a wide range of concentrations. Pronounced line broadening in $^{1}H,^{15}N$-HSQC NMR spectra and failure to assign peaks corresponding to the carboxy-terminal helix 4 of Elc1 indicated that helix 4 is conformationally labile. Measurement of ^{15}N NMR relaxation parameters including T_1, T_2, and the $\{^{1}H\text{-}^{15}N\}$ nuclear Overhauser effect revealed (i) surprisingly high flexibility of residues 69−77 in loop 5, and (ii) chemical exchange contributions for a large number of residues throughout the protein. Addition of 2,2,2-trifluoroethanol (TFE) stabilized helix 4 and reduced chemical exchange contributions, suggesting that stabilization of helix 4 suppresses the tendency of Elc1 to undergo conformational exchange on a micro- to millisecond time scale. Binding of a peptide representing the major ELC binding site of the von Hippel−Lindau (VHL) tumor suppressor protein almost completely eliminated chemical exchange processes, but induced substantial conformational changes in Elc1 leading to pronounced rotational anisotropy. These results suggest that elongin C interacts with various target proteins including the VHL protein by an induced fit mechanism involving the conformationally flexible carboxy-terminal helix 4.

Targeted protein degradation via the ubiquitin−proteasome pathway plays an important role in a wide variety of cellular processes, including cell-cycle progression, signal transduction, transcriptional activation, and many others (*1*−*3*). Ubiquitylation of target proteins involves a cascade of three enzymatic activities (*3*, *4*): a ubiquitin-activating enzyme (E1), a ubiquitin-conjugating enzyme (E2), and a ubiquitin ligase (E3). The CBC^{VHL} multiprotein complex is a recently discovered mammalian E3 ubiquitin ligase (*5*−*7*) composed of elongin C (ELC),[1] elongin B (ELB), cullin-2, Rbx1/Roc-1, and the von Hippel−Lindau (VHL) tumor suppressor protein (*8*−*10*). The *VHL* gene is mutated in the familial cancer syndrome von Hippel−Lindau disease as well as in spontaneous malignancies (*11*). Many of the cancer-associated *VHL* mutations have been shown or are predicted to interfere with CBC^{VHL} complex formation and/or function (*12*), suggesting that one important mechanism of tumor suppression by the VHL protein is the control of target protein levels via ubiquitylation and proteasomal degradation.

The architecture of CBC^{VHL} resembles that of the better characterized SCF (*S*kp1-*C*dc53/cullin-*F* box protein) family of E3 ubiquitin ligases (*13*−*16*): Rbx1/Roc-1 is a common subunit of both E3 families (*10*, *17*), and ELC and cullin-2 are homologues of Skp1 and Cdc53/cullin-1, respectively (*8*, *18*). In the case of SCF complexes, a great diversity in substrate−protein interactions is achieved via variable F box protein subunits, which function as targeting modules by simultaneously binding to the Skp1 subunit and substrate proteins (*13*, *16*, *18*). For CBC complexes, a similar diversity of substrate proteins remains to be established. ELC/ELB interact in vivo not only with VHL but also with other so-called BC box proteins including elongin A (*19*) and proteins of the SOCS box family (*20*, *21*). This suggests that BC box proteins may deliver an as yet largely unknown set of substrate proteins to CBC complexes, thus paralleling F box proteins in SCF complexes.

The recently solved crystal structure of the human VHL/ELC/ELB complex (*12*) was the first step toward understanding at molecular detail the architecture and function of CBC and SCF ubiquitin ligases. ELC is the central component of the VHL/ELC/ELB complex. It possesses a β-β-α-α-β-α-α topology of secondary structure elements (Figure 1). Helices 3 and 4 are separated by the long loop 5 that, in the context of the crystal, is well-ordered and in an extended conformation. ELC has two distinct, largely hydrophobic

† This work was supported in part by EMBO long-term fellowship ALTF 220-1997 to A.B.

* Corresponding author. Phone: 0044-29-2052-6429; Fax: 0044-29-2052-6206; email: mark.howard@eu.biotech.com.

‡ MRC Centre for Protein Engineering.

§ Present address: Amersham Pharmacia Biotech Ltd., Cardiff Laboratories, Forest Farm, Whitchurch Cardiff, Wales, CF14 7YT, UK.

|| MRC Laboratory of Molecular Biology.

[1] Abbreviations: TFE, 2,2,2-trifluoroethanol; DTT, dithiothreitol; Elc1, yeast elongin C; ELC, mammalian elongin C; ELB, elongin B; VHL, von Hippel−Lindau protein; CBC, cullin2−elonginB−elongin C complex; HIF, hypoxia-inducible transcription factor; HSQC, heteronuclear single quantum correlation; NOE, nuclear Overhauser effect; NOESY, NOE spectroscopy; TOCSY, total correlation spectroscopy.

10.1021/bi0008231 CCC: $19.00
Published on Web 08/12/2000

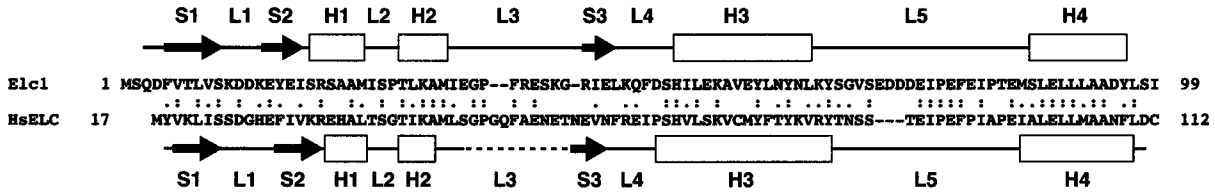

FIGURE 1: Structural organization of elongin C. The plot shows an alignment of Elc1 and residues 17−112 of human ELC (HsELC), prepared with ClustalW (MacVector, Oxford Molecular). Identical and similar residues are indicated by colons and dots, respectively. The secondary structure of Elc1 derived from chemical shift analysis (see Supporting Information) is indicated on top of the alignment. The secondary structure of human ELC (*12*) is shown below the alignment. Arrows, strands; open boxes, helices; broken line, disordered segment in the crystal structure of human ELC.

binding sites for VHL and ELB, respectively: The three β strands form an intermolecular β sheet with ELB. The carboxy-terminal helix 4 complements three α helices in VHL to form an intermolecular four-helix cluster, which is supplemented by additional contacts between VHL and residues in loop 5 of ELC.

We are interested in the structural and dynamic properties of ELC in solution, which enable it to interact with different BC box proteins including VHL. To this end, we are studying the homologous Elc1 protein from the baker's yeast *Saccharomyces cerevisiae* (*22*). The overall homology between Elc1 and human ELC is high, with 18% identical and 33% similar residues (*12*) (Figure 1). Although yeast does not possess ELB or VHL homologues, Elc1 has been shown to bind human VHL (*22*). Yeast may therefore provide a simple model for analyzing interactions between elongin C and BC box proteins.

In a recent NMR study, Botuyan and co-workers investigated the interaction of Elc1 with three different (poly-) peptides including a VHL-derived peptide representing the major ELC binding site of VHL (*23*). Based on a qualitative assessment of ^{1}H,^{15}N-HSQC spectra and on analytical ultracentrifugation data, they concluded that free Elc1 forms homotetramers composed of subunits with a structured N-terminal region and a dynamically unstable C-terminal region, whereas the Elc1·VHL-peptide complex undergoes structural rearrangements and dissociation into homodimers. In this study, we present a quantitative analysis of Elc1 backbone dynamics in the free and peptide-bound state by NMR relaxation measurements. In addition, we show rigorously by a combination of analytical ultracentrifugation and size exclusion chromatography that free Elc1 is a monomer of nonglobular shape.

MATERIALS AND METHODS

Materials. Bovine thrombin (T-6634) was from Sigma (St. Louis). VHL peptide (NH_2-TLKERCLQVVRSLVK-CO_2H), corresponding to residues 157−171 of human VHL, was obtained from Oswel Research Products Ltd. (Southampton). The lyophilized peptide was resuspended in 5% acetonitrile and brought to neutral pH with NaOH. The solution was extensively dialyzed against 1% acetonitrile and, subsequently, buffer A (50 mM sodium phosphate, pH 6.8, 150 mM NaCl, 0.05% NaN_3) containing 10 mM DTT and 1% acetonitrile. The peptide was flash-frozen and stored at −20 °C. The identity of the peptide was verified by mass spectroscopy and quantitative amino acid analysis. The concentration of the stock solution was determined by quantitative amino acid analysis to be 9 mM.

Cloning Procedures. The gene encoding Elc1 was amplified from genomic yeast DNA (Promega) by standard PCR protocols using the primer pair 5′-CGGGATCCCAAGATTTCGTTACGTTAGTATC-3′ (forward primer) and 5′-GGGAATTCTTATATACTCAAATAGTCCGCCGCAAG-3′ (backward primer). The coding sequence for Elc1 was slightly changed by the introduction of a *Bam*HI restriction site at the 5′-end, resulting in a single methionine-to-glycine amino acid exchange at residue 1. The purified PCR product was subcloned via *Bam*HI and *Eco*RI restriction sites into pHisGroE, a pRSETa (Invitrogen) derivative coding for cleavable N-terminal fusions with a $(His)_6$-tag and an apical domain fragment of GroEL (M. Proctor and A. R. Fersht, unpublished results). Sequencing of both strands of the subcloned insert confirmed that codon 63 codes for asparagine (Genbank accession no. 6325211), not tyrosine (Genbank accession no. BAA22612).

Expression and Purification of Elc1. Escherichia coli C41(DE3) cells (*24*) were transformed with pHisGroE(Elc1) and grown in 2×YT medium containing 100 μg/mL ampicillin at 25 °C. At mid-log phase, overexpression of $(His)_6$-GroE-Elc1 fusion protein was induced by addition of isopropyl-D-thiogalactoside (0.2 mM final concentration) for 16 h. Uniformly ^{15}N- and $^{15}N/^{13}C$-labeled Elc1 was produced by growing cells in M9 minimal media containing $^{15}NH_4Cl$ and/or $[^{13}C_6]$glucose as sole nitrogen and carbon sources, respectively.

Harvested cells were resuspended in 20 mM sodium phosphate, pH 7.4, 150 mM NaCl and lysed by two rounds of sonication on an EmulsiFlex-C5 high-pressure homogenizer (Avestin, Ottawa). The cell debris was removed by centrifugation, and the supernatant was applied to Ni-NTA-agarose beads (Qiagen) equilibrated in 20 mM sodium phosphate, pH 7.4, 150 mM NaCl, 10 mM imidazole. After repeated washes with this buffer, Elc1 was liberated by thrombin cleavage overnight at room temperature, and further purified by size exclusion chromatography on a Superdex S75 26/60 column (Amersham Pharmacia Biotech) in buffer A. The protein was dialyzed against buffer A, flash-frozen, and stored at −70 °C. The identity of the purified protein was verified by mass spectrometry and quantitative amino acid analysis. Mass spectrometry confirmed the predicted molecular mass of this construct of 11 253 Da. On the basis of amino acid analysis, the molar extinction coefficients in buffer A were determined to be $\epsilon_{276\ nm} = 6919$ L/(mol·cm), $\epsilon_{280\ nm} = 6236$ L/(mol·cm), $\epsilon_{284\ nm} = 5353$ L/(mol·cm), and $\epsilon_{287\ nm} = 3212$ L/(mol·cm).

Analytical Ultracentrifugation. Sedimentation analysis was performed in buffer A at 25 °C with initial protein concentrations ranging from 75 to 300 μM in a Beckman XL-I

analytical ultracentrifuge, equipped with An-60Ti (velocity sedimentation) and An-50Ti (equilibrium sedimentation) rotors, respectively, using 12 mm standard double sector cells, and scanning at 280 nm (velocity sedimentation) and 280, 284, and 287 nm (equilibrium sedimentation). Sedimentation equilibrium experiments were performed at 12 000, 15 000, and 18 000 rpm, with initial overspeeding at 1.5-fold speed for 6 h to accelerate the attainment of equilibrium (*25*). Subsequently, scans were taken at intervals of 24 h until two successive scans superimposed exactly, when the later scan was taken as being operationally at equilibrium. Data were analyzed by taking overlapping sets of 41 data points to calculate the apparent weight average molecular mass, taken to be at the concentration of the middle point, and calculating $\bar{M}_{w,app}$ for each set by nonlinear regression with the equation (*26*):

$$\bar{M}_{w,app} = \frac{d\ln(c)}{dr^2}\frac{2RT}{\omega^2(1-\phi'\rho_0)}$$

where $\bar{M}_{w,app}$ is the apparent weight average molecular mass, c is the concentration (as optical density) at radius r, ω is the angular velocity (in radians/s), ϕ' is the apparent partial specific volume, and ρ_0 is the solvent density. These latter two parameters were measured using an oscillating densitometer (*27*) (model DMA60 with a DMA602 cell; Anton Paar, Graz, Austria) to measure the density of solvent (ρ_0) and solution. The protein concentration (∂c_2) was determined by amino acid analysis and together with the density difference ($\partial\rho$) allowed the density increment to be determined and hence ϕ' calculated from the equation (*26*):

$$\left(\frac{\partial\rho}{\partial c_2}\right)_\mu = 1-\phi'\rho_0$$

Alternatively, the equilibrium sedimentation data were analyzed directly by a global fitting procedure to a model for self-associating systems, as defined in the Beckman implementation of the Microcal Origin software provided with the ultracentrifuge. Fitted parameters included the following: mass of the monomeric species M, protein concentration at reference radius c_0, absorbance offset, stoichiometry of ith self-associated species N_i, and association constant $K_{a,abs}$ (in absorbance units) for the equilibrium between M and N_i. Absorbance-based association constants were converted to concentration-based association constants $K_{a,conc}$ using the equation (*28*):

$$K_{a,conc} = K_{a,abs}\times\left(\frac{1.2\times\epsilon}{2}\right)$$

where ϵ is the molar extinction coefficient. $K_{a,conc}$ values for dimer formation were inverted to obtain the corresponding K_d values (in mol/L).

Sedimentation velocity experiments were performed at 60 000 rpm, and scans were taken as rapidly as possible (approximate 4.5 min intervals) over a period of 4 h. Sedimentation coefficients were determined from the maximum of plots of $g(s^*)$ against s^*, where $g(s^*)$ is the fraction of material sedimenting between s^* and $(s^*+\delta s^*)$ (*29*, *30*), using the DCDT+ software package (version 1.05) (*31*). This software was also used for direct fitting of simple Gaussian functions to dc/dt versus s curves, to determine molecular mass directly from sedimentation velocity (*32*). Models with one and two species present were tested. The correction from s^* to $s_{20,w}$ was based on experimentally determined values for ϕ' and ρ_0 (see above) and a viscosity of 0.8905 cP, calculated with SEDNTERP (version 1.03) (*33*).

Size Exclusion Chromatography. Fifty microliters of Elc1 (5−440 μM) or molecular mass standards was loaded onto a Superdex 75 HR 10/30 column (Amersham Pharmacia Biotech) and eluted at room temperature at a flow rate of 0.75 mL/min with buffer A. Elution of proteins was monitored at 280 nm. The distribution coefficient K_{av} (*34*, *35*) for the different proteins was calculated according to

$$K_{av} = \frac{(V_e - V_0)}{(V_t - V_0)}$$

where V_t is the total column volume (24 mL), V_0 is the void volume as defined by the elution volume of Blue Dextran, and V_e is the elution volume of a given solute.

NMR Sample Preparation. Uniformly ^{15}N- and ^{15}N/^{13}C-labeled Elc1 was filtered through a 100 nm syringe top filter, dialyzed overnight against buffer A containing 5% D_2O, and concentrated to 300−400 μM final concentration in an Amicon concentrator. Complexes between VHL peptide and Elc1 were formed by adding a 2-fold molar excess of peptide to a ^{15}N-labeled Elc1 sample. Complex formation was verified by the observation of substantial chemical shift changes in ^{1}H,^{15}N-HSQC spectra upon addition of peptide. Subsequently, the Elc1·peptide complex was recovered, dialyzed overnight against buffer A containing 5% D_2O and 10 mM DTT, and used for further NMR experiments.

NMR Spectroscopy. Spectra were recorded at 298 K on Bruker AMX 500 and DRX 600 NMR spectrometers. ^{1}H,^{15}N-HSQC experiments with WATERGATE water suppression (*36*) were obtained for ^{15}N-labeled Elc1 samples in the absence and presence of 10% TFE or VHL peptide, respectively. Sequence-specific resonance assignments for ^{15}N/^{13}C-labeled Elc1 were made based on the following triple-resonance experiments: HN(CO)CA, HNCA (*37*), CBCA(CO)NH (*38*), HNCACB (*39*). Sequence-specific resonance assignments for ^{15}N/^{13}C-labeled Elc1 in the presence of 10% TFE were made based on a HNCACB experiment. Pairs of ^{15}N-NOESY−HSQC and ^{15}N-TOCSY−HSQC experiments were acquired for ^{15}N-labeled Elc1 in absence and presence of 10% TFE to confirm and extend sequential assignments.

Data were processed and analyzed with Felix97 (MSI). Typically, shifted sinesquare window functions were applied before Fourier transformation. Data were zero-filled 2-fold in all dimensions. In 3D experiments, linear prediction was performed in the ^{15}N dimension and, where applicable, ^{13}C dimension. ^{15}N-NOESY−HSQC and ^{15}N-TOCSY−HSQC data were analyzed with Ansig3 (*40*).

^{15}N T_1, T_2, and {^{1}H-^{15}N} NOE experiments (*41*) were recorded at a ^{15}N frequency of 50.13 MHz on a Bruker AMX500 spectrometer. T_1 relaxation delays were set to 16, 32, 48, 80, 120, 200, 280, 360, 440, 520, 600, 760 ms (absence of TFE); 16, 88, 160, 232, 304, 376, 448, 520, 592, 664, 736, 808 ms (presence of TFE); and 16, 80, 160, 240, 320, 400, 480, 600, 720, 840, 1000, 1200 ms (Elc1·VHL peptide complex). T_2 experiments featured an CPMG pulse train with a spin−echo delay, 2τ, of 1.25 ms. T_2 relaxation

delays were set to 10, 20, 30, 40, 50, 70, 90, 110, 130, 160, 190, 200, 220, 230 ms (absence of TFE); 10, 20, 40, 60, 80, 100, 120, 140, 160, 180, 200, 240 ms (presence of TFE); and 10, 20, 40, 60, 80, 100, 120, 140, 160, 180, 200, 220, 240 ms (Elc1·VHL peptide complex). Peak volumes were fitted to a monoexponential decay function using KaleidaGraph 3.0 (Abelbeck Software). The standard errors from the Levenberg−Marquardt fitting routine were taken as the uncertainties in the obtained T_1 and T_2 values, and were typically 5−10% of the T_1 and T_2 values. The actual standard errors are given as Supporting Information. {^{1}H-^{15}N} NOEs were determined from spectra obtained with and without presaturation of amide proton resonances. Presaturation was achieved by applying WALTZ-16 composite pulse decoupling with a field strength of 1 kHz for 2 s. Reference spectra were obtained by replacing the presaturation sequence with off-resonance continuous wave decoupling or a simple delay. For both experiments, the recycle delay was set to 5 s. The NOE values were calculated according to the formula:

$$\mathrm{NOE} = I'/I_0$$

where I' and I_0 are the peak intensities in the spectrum with and without presaturation, respectively. Experimental errors were estimated from the rms noise of the spectra (*42*) and were approximately 30% for the Elc1·VHL peptide complex, and significantly higher for free Elc1 in the absence or presence of TFE due to spectral overlap and the poor sensitivity of the experiments under these experimental conditions.

RESULTS

Elc1 Is a Monomer. To characterize the structure and conformational flexibility of Elc1 in solution, a range of NMR experiments was performed. However, initial ^{1}H,^{15}N-HSQC spectra obtained at Elc1 concentrations of 0.8−1.1 mM displayed excessive line broadening (data not shown), suggesting that Elc1 self-associates at these concentrations. NMR line widths decreased as the concentration was reduced from 0.8 to 0.45 mM, and remained largely constant at concentrations between 0.45 and 0.1 mM. Elc1 has been reported to exist as a mixture of tetramers and dimers at concentrations of 0.7−1.5 mM (*23*), whereas the homologous Skp1 protein forms monomers and dimers (*43*). As a prerequisite to our NMR analyses, we therefore chose to rigorously clarify the oligomeric state of Elc1 by analytical ultracentrifugation. The calculations of the apparent molecular mass of Elc1 were based on experimentally determined values for solvent density (ρ_0) and apparent partial specific volume (ϕ') of 1.008618 g/mL and 0.7328 mL/g, respectively.

Sedimentation velocity experiments were performed at 150 μM initial protein concentration for several hours, allowing for the complete separation of the boundary from the meniscus (Figure 2a). Ten consecutive scans between 135 and 180 min sedimentation were used for calculating the apparent sedimentation coefficient distributions [$g(s^*)$] according to the time-derivative method (*29, 30*) (Figure 2b). The apparent sedimentation coefficient distributions exhibited a single maximum around 1.2 S, compatible with a single species. The dc/dt data were fitted to the Svedberg equation to give values for $s_{20,w}$ of 1.289 (±0.003) S and a molecular mass of 11.6 (±0.12) kDa. These values correspond very well to a monomer of Elc1 (theoretical molecular mass 11.253 kDa). Very similar results were obtained upon fitting different sets of 10 consecutive scans at 75 or 150 μM initial protein concentration. The fitted molecular masses were consistently in the range of 10.5−13.5 kDa. To investigate whether the distribution of s^* truly reflects the presence of a single protein species, we tried to fit the various sets of dc/dt data to a two-species model by randomly choosing an initial estimate for s^* of the second species. In most cases, the fitting process did not converge, indicating that the experimental data are inconsistent with the presence of a second distinct species. In some cases, the fitting procedure converged to result in apparent molecular masses for the second species in the range of 85−165 kDa. If these results are not artifacts of the fitting procedure but rather reflect the presence of a second Elc1 species, then this species appears to be an oligomer of 8−16 subunits, most likely some soluble aggregate. From the fitting results for the concentration (as absorption) of this second species, its relative abundance can be estimated to be no more than 2.5% of the sample.

To determine the apparent molecular mass of Elc1 directly, we performed sedimentation equilibrium experiments at different initial Elc1 concentrations and three different rotor speeds (12 000, 15 000, and 18 000 rpm). The data were analyzed by two different methods. First, we plotted the mass average apparent molecular weights as a function of protein concentration (Figure 2c,d). Datasets from four different initial protein concentrations overlapped and showed a plateau at an apparent molecular mass of approximately 11 kDa. The best fit for the data was obtained with a model for a single, monomeric species without nonideality. Extrapolation of this curve fit to zero concentration resulted in an apparent mass of 11 355 (±70) Da, in excellent agreement with the calculated molecular mass of Elc1. Most importantly, there is no indication of a dimeric subpopulation at protein concentrations as high as 3 mg/mL (270 μM), similar to the concentrations used in our NMR experiments. Second, we subjected the various datasets directly to a global fitting procedure to a mathematical model for a self-associating system with up to four different oligomeric species (data not shown). Again, the data fitted well to give apparent molecular masses of 10.3−11.8 kDa. As in the case with the sedimentation velocity data, we could not satisfactorily fit the data to a model including a dimeric or multimeric species. In cases where the fitting procedure converged, the fitted absorption-based association constants were converted to thermodynamic dissociation constants (K_d's) in the millimolar range, from 6 to over 100 mM. The lowest of these K_d values was then used to calculate a potential oligomeric subpopulation of less than 3.5% even at the highest concentrations used in NMR experiments.

Taken together, these results demonstrate that Elc1 is predominantly, if not exclusively, monomeric up to almost half-millimolar concentrations, with no evidence for oligomerization. The results do not allow us to completely rule out the existence of oligomeric subspecies, but set an upper limit of 3.5% for their abundance and suggest that they represent unspecific assemblies rather than a defined subpopulation.

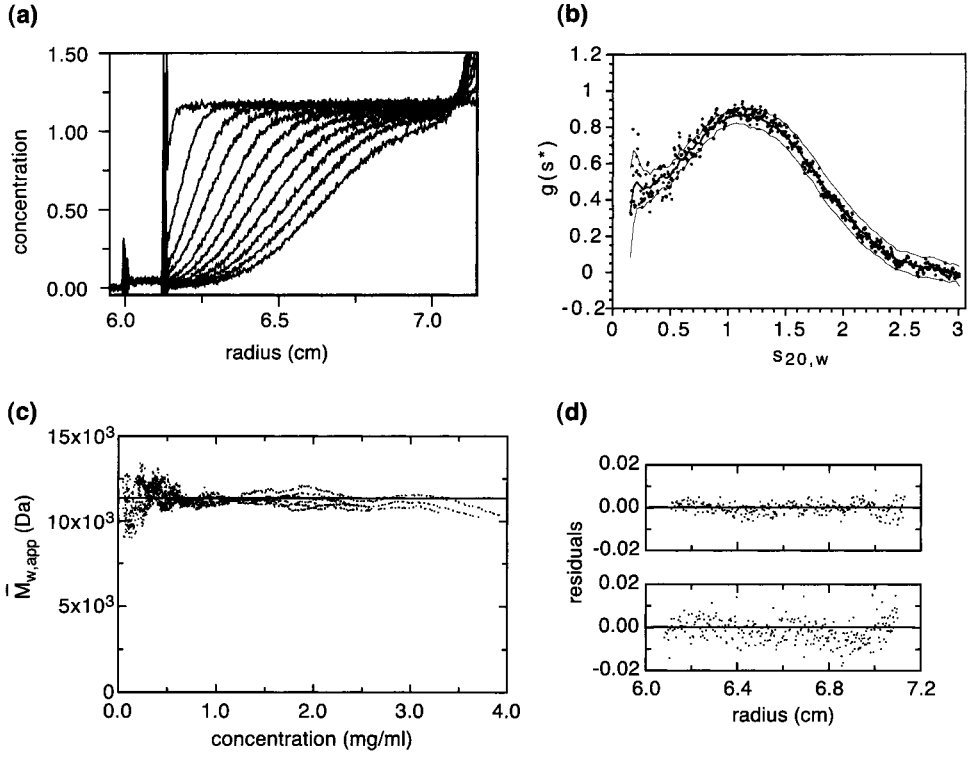

FIGURE 2: Analytical ultracentrifugation of Elc1. (a, b) Sedimentation velocity analysis. Elc1 (150 μM) was sedimented at 60 000 rpm in a Beckman XL-I analytical ultracentrifuge equipped with an An-60Ti rotor. (a) Overview of the boundary movement. 65 scans taken at intervals of ca. 4.5 min are plotted as concentration (in absorption units) against cell radius. For clarity, only every fifth scan is shown. (b) Distribution of apparent sedimentation coefficients. Ten scans taken between 135 and 180 min were analyzed using the time derivative method (*29*, *30*). Shown are the calculated $g(s^*)$ values (dots), a smoothed curve fit to the data points (thick line), and smoothed curve fits for the standard deviation of the data points (thin lines). (c, d) Sedimentation equilibrium analysis. Elc1 at different initial concentrations [75 μM, 150 μM (duplicates), 225 μM (duplicates), and 300 μM (duplicates)] was centrifuged at 18 000 rpm in a Beckman XL-I analytical ultracentrifuge equipped with an An-50Ti rotor until two subsequent scans taken at 24 h intervals overlapped completely. (c) Plot of the apparent weight average molecular mass against Elc1 concentration. Data from all seven samples are plotted together, to demonstrate the extent of overlap. The best fit for all data to a model for one ideal monomeric species is shown as a solid line. It extrapolates to an apparent mass at zero concentration of 11 355 (±70) Da. (d) Residual errors between the measured optical density and that calculated from fitting to a model for one ideal monomeric species for samples at 150 μM (bottom panel) and 225 μM (top panel) initial concentration, respectively.

The analytical ultracentrifuge experiments were complemented by analytical size exclusion chromatography, i.e., a methodology that is sensitive to both molecular mass and shape of the solute (see Supporting Information). Elc1 at loading concentrations between 5 and 440 μM eluted with an apparent molecular mass of ca. 20.7 kDa, as calculated from the curve fit for a set of globular standard proteins. Because Elc1 in the concentration range tested was at least 96% monomeric according to the analytical ultracentrifuge analyses, we conclude that its aberrant elution behavior is caused by a nonglobular shape.

Backbone Dynamics. Since Elc1 at concentrations up to 450 μM exists as a predominantly monomeric species, all NMR experiments were performed at concentrations between 300 and 400 μM. Even under these conditions, ^{1}H,^{15}N-HSQC spectra of Elc1 were characterized by pronounced spectral overlap, variable peak intensities, and the absence of a number of peaks (Figure 3a). These factors prevented the assignment of 30% of the backbone resonances of Elc1, the majority of which corresponded to carboxy-terminal residues forming loop 5 and helix 4 (Figure 1). Whereas the NMR spectra suggest conformational flexibility of residues 80−99, they are inconsistent with a highly flexible random coil conformation, because no correspondingly sharp, intense peaks were detected. To possibly stabilize helix 4, we added to the NMR samples 2,2,2-trifluoroethanol (TFE), which is known to stabilize helical structure in peptides (*44*−*47*) and proteins (*48*). In the presence of 10% TFE, significantly improved NMR spectra were obtained (Figure 3b). In particular, line widths decreased, the resolution in the central region of the HSQC spectrum increased substantially, and additional peaks were observable. Notably, the majority of chemical shifts of the backbone amide (Figure 3) and H_α, C_α, and C_β resonances (Supporting Information) remained unchanged, indicating that the structural organization of Elc1 was not affected by the presence of 10% TFE. The improved spectra allowed the unambiguous assignment of 14 additional peaks including several corresponding to residues in helix 4, in total 85% of all Elc1 backbone residues.

Based on these assignments, the backbone dynamics of Elc1 in the absence and presence of TFE were analyzed by measurement of longitudinal (T_1) and transverse (T_2) relaxation times as well as {^{1}H-^{15}N} heteronuclear NOEs. Whereas longitudinal and transverse relaxation behavior is governed by several parameters including internal flexibility and chemical exchange, heteronuclear NOE values reflect mainly internal dynamics of amide N−H vectors (*49*). In the absence of TFE, Elc1 exhibited a relatively uniform distribution of T_1 values (average 0.515 ± 0.049 s; Figure 4a), with residues 68−77 in loop 5 possessing slightly higher values up to 0.6 s. In contrast, the transverse (T_2) relaxation times varied greater, ranging from shorter than 0.05 s to

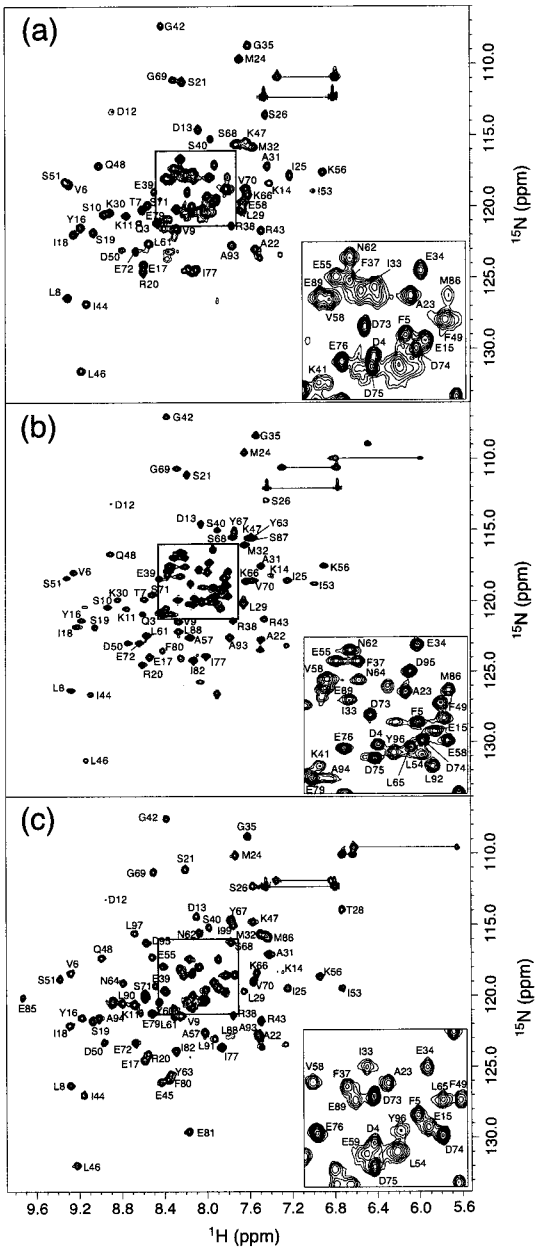

FIGURE 3: ^{1}H,^{15}N-HSQC spectra of Elc1. (a) Free Elc1 in the absence of TFE. (b) Free Elc1 in the presence of 10% TFE. (c) Elc1·VHL peptide complex. All spectra were recorded at 25 °C and final sample concentrations of 350 μM. Assigned backbone amide resonances are labeled; assignments for the Elc1·peptide complex are taken from (*23*). Horizontal lines indicate pairs of side chain resonances. The insets show magnifications of the central regions of the spectra.

0.22 s (average 0.096 ± 0.041 s; Figure 4b). Remarkably, residues 68−77 displayed by far the highest T_2 values, indicating strongly increased flexibility. Residues 39 and 40 in loop 3 also possessed T_2 values above average. The lowest T_2 values were measured for residues K14, S26, L29, L61, M86, and A93, consistent with the significant line broadening observed for the corresponding peaks (Figure 3a). The internal mobility of Elc1 backbone amide vectors was assessed by measurement of heteronuclear NOEs. The accuracy of the obtained experimental data was restricted by considerable spectral overlap in combination with poor sensitivity due to the low protein concentration used. Therefore, the results were only examined qualitatively for consistency with the other relaxation data. The majority of Elc1 residues exhibited {^{1}H-^{15}N} NOE values between 0.4 and 0.8 (Figure 4c), indicating low intrinsic flexibility for those regions of Elc1 with regular secondary structure. In contrast, the significantly lower NOE's ranging from 0.3 to −0.05 highlight strong internal motions of residues 68−77 in loop 5, in good agreement with the high T_2 values for these residues. Taken together, these results demonstrate a pronounced flexibility on the nanosecond to picosecond time scale of the first half of loop 5, which was not anticipated from the crystal structure of human ELC. In addition, the relaxation data for those residues in helix 4 that could be assigned are similar to those in the other secondary structure elements of Elc1, thus suggesting the presence of residual structure for helix 4.

In the presence of 10% TFE, a slight increase in T_1 values (average 0.586 ± 0.048 s) was observed (Figure 4d), possibly reflecting the different solvent conditions. The average T_2 value (0.098 ± 0.039 s) was not significantly different in the presence of 10% TFE, and also on an individual residue basis most changes in T_2 were small (Figure 4e). Two notable exceptions are residues M86 and A93 in helix 4: their T_2 values increased significantly, from 0.030 ± 0.006 and 0.052 ± 0.005 s, respectively, in the absence of TFE, to 0.070 ± 0.001 and 0.079 ± 0.001 s, respectively, in the presence of TFE. These increased T_2 values probably reflect a reduced chemical exchange contribution to transverse relaxation mechanisms in the presence of TFE (see below). The high internal flexibility of loop 5 was retained under these conditions, as indicated by the high T_2 and low hetNOE values (Figure 4e,f). Again, the relaxation parameters for residues in helix 4 were well within the average for the entire protein, indicating that this part of Elc1 does not possess higher internal flexibility than the other regions of defined secondary structure.

To further analyze the relaxation behavior of Elc1 in the absence and presence of TFE, we compared the experimentally determined T_1 and T_2 values with theoretically calculated parameters for fast internal motion based on the model-free formalism of Lipari and Szabo (*50*). In this formalism, the spectral density functions underlying the experimentally determined relaxation parameters are expressed as a function of the generalized order parameter, S^2, the effective correlation time describing internal motions, τ_e, and the total rotational correlation time, τ_m. S^2 is a measure of the spatial restriction of fast internal motions: at its maximum ($S^2 = 1.0$), no fast internal motions occur. A plot of T_1 versus T_2 demonstrated a pronounced spread of T_2 values, with many data points outside the calculated contour for $S^2 = 1.0$ (Figure 5a). This indicates that contributions from chemical exchange phenomena, which manifest as reduced T_2 values, play a significant role for the relaxation mechanism of a large fraction of Elc1 residues. At the range of high T_2 values, the data points for residues 69−77 fall between the contours for $S^2 = 0.8$ and $S^2 = 0.6$, confirming the occurrence of fast internal motions in the first half of loop 5. In the presence of TFE, the data points again spread much more along the T_2 than along the T_1 axis (Figure 5b). However, compared to the absence of TFE, a higher proportion of points falls between $S^2 = 0.8$ and $S^2 = 1.0$ or only slightly outside the contour for $S^2 = 1.0$, demonstrating that pronounced chemical exchange is restricted to a smaller subset of residues.

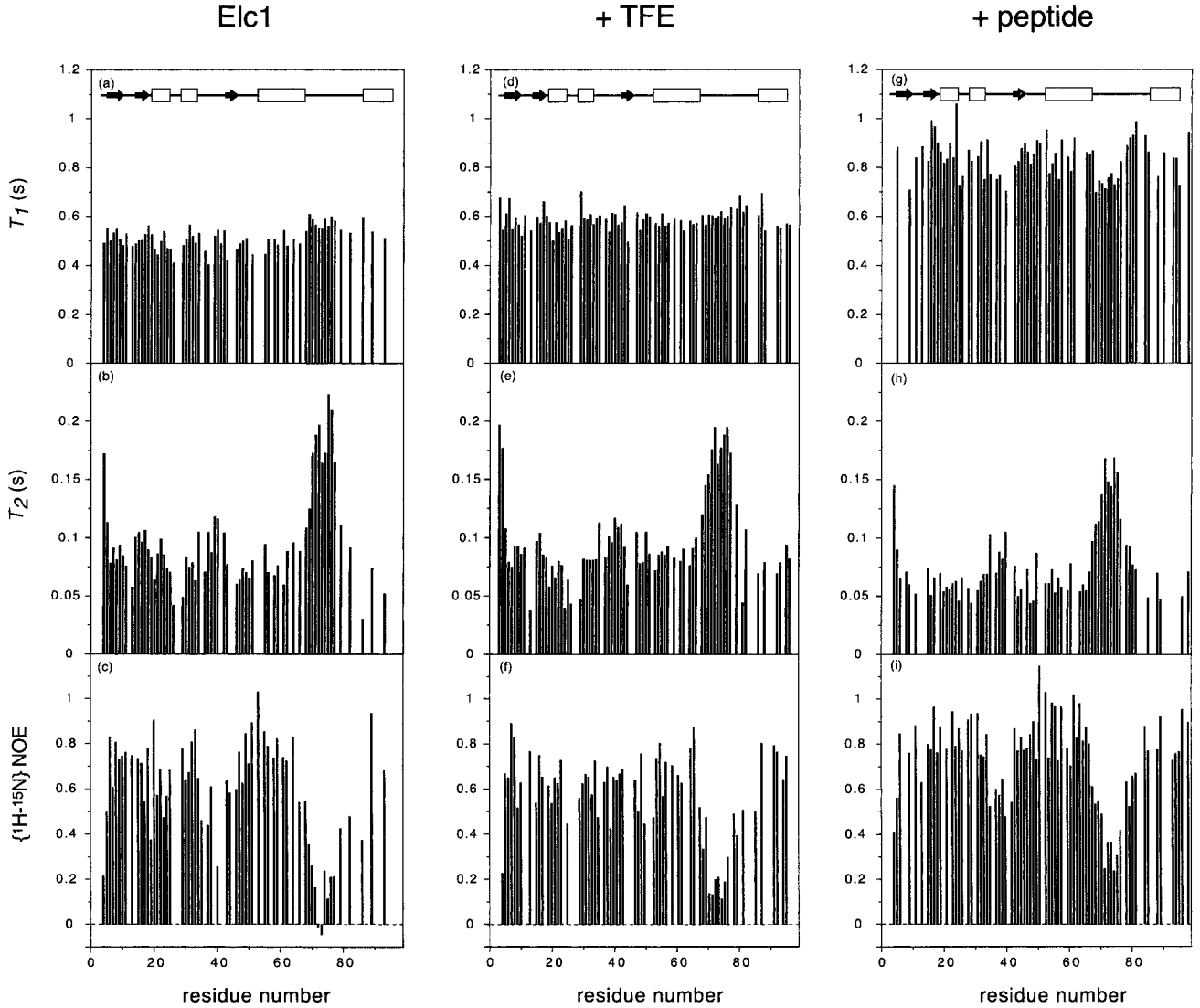

FIGURE 4: Backbone dynamics of Elc1. (a−c) Free Elc1 in the absence of TFE. (d−f) Free Elc1 in the presence of 10% TFE. (g−i) Elc1·VHL peptide complex. (a, d, g) Longitudinal relaxation time, T_1; (b, e, h) transverse relaxation time, T_2; (c, f, i) {^{1}H-^{15}N} heteronuclear NOEs as I'/I_0, where I' and I_0 are the peak intensities in the presence and absence of presaturation, respectively. The secondary structure of Elc1 is indicated at the top of panels a, d, and g.

For example, several of the data points with strong chemical exchange contributions correspond to residues 24−29, within and neighboring loop 2. This suggests that in the presence of TFE chemical exchange affects few defined structural elements rather than the overall structure of Elc1. Interestingly, residues M86 and A93 in helix 4, which exhibited strong chemical exchange contributions in the absence of TFE, experienced significantly reduced chemical exchange in the presence of TFE: the corresponding data points moved from far outside $S^2 = 1.0$ to the group of data points only slightly outside $S^2 = 1.0$.

In summary, the measurements of backbone dynamics (i) confirm the existence of stable secondary structure elements, (ii) reveal the presence of a highly flexible region spanning residues 68−79 in loop 5, (iii) reveal pronounced chemical exchange contributions to experimental T_2 values that are reduced in the presence of TFE, and (iv) suggest different relaxation mechanisms for residues in helix 4 in the absence and presence of TFE.

Peptide Binding. Both human ELC and Elc1 form stable complexes with VHL (*12*, *22*) or a VHL-derived peptide spanning helix 1 of VHL (*23*, *51*). The crystal structure of the human VHL/ELC/ELB complex suggests that helix 4 of ELC (and Elc1) is stabilized by interaction with helix 1 of VHL. It has indeed been demonstrated that binding of VHL peptide leads to substantial changes in the ^{1}H,^{15}N-HSQC spectrum of Elc1, suggesting peptide-induced conformational changes (*23*). However, changes in chemical shift cannot be directly equated with changes in structure. We therefore investigated the effect of peptide binding on conformation and flexibility of Elc1 by analyzing the backbone dynamics of the Elc1·peptide complex.

Binding of VHL peptide led to changes in the ^{1}H,^{15}N-HSQC spectrum of Elc1 which were basically identical to those described by Botyuan et al. (*23*); i.e., almost all expected backbone resonances and four pairs of side chain resonances were observed, with many residues throughout Elc1 possessing altered amide chemical shifts (Figure 3c). In addition to these effects, peptide binding also caused a marked change in relaxation behavior (Figure 4g−i): In comparison to free Elc1 in the absence or presence of TFE, the T_1 values were strongly increased, to an average value

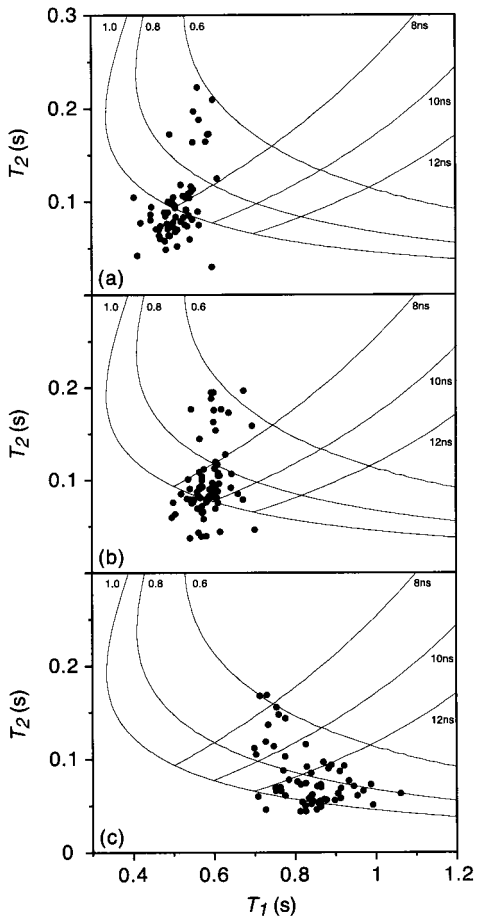

FIGURE 5: Plot of experimental T_1 against experimental T_2 values for Elc1. (a) Elc1 without TFE; (b) Elc1 in the presence of 10% TFE; (c) Elc1·VHL peptide complex. Each data point corresponds to one residue of Elc1. Superimposed are two sets of contours calculated with the spectral density functions of the model-free formalism (*50*). The contours labeled at the top axis represent fixed values of the order parameter S^2 for varying total correlation times τ_m. Conversely, the contours labeled at the right-hand axis represent fixed values of τ_m for varying values of S^2. All calculations are based on an internal correlation time τ_e of 50 ps.

of 0.840 ± 0.092 s, whereas the T_2 values were decreased slightly (average value 0.077 ± 0.031 s). The heteronuclear NOE values in the presence of peptide were slightly higher on average, indicating a more rigid overall structure of the Elc1·peptide complex. Both T_2 and heteronuclear NOE values again highlight the pronounced flexibility of the first half of loop 5, which, however, appeared somewhat reduced in comparison to free Elc1. In addition, the T_2 and particularly heteronuclear NOE data revealed significant flexibility for residues 36−40 in loop 3. In the absence of peptide, a similar flexibility for loop 3 had been suggested by the T_2 data but had to remain unconfirmed because of the insufficient quality of the heteronuclear NOE data for that region (Figure 4b,e).

The most dramatic effect of peptide binding was revealed upon plotting the T_1 and T_2 values of the Elc1·peptide complex against each other (Figure 5c). In contrast to free Elc1 in the absence or presence of TFE, the data points were widely spread along the T_1 axis, with T_1 values ranging from 0.7 to almost 1.1 s. This spread indicates a pronounced rotational anisotropy of the Elc1·peptide complex which is also reflected by an increase in the apparent rotational correlation time from roughly 9 ns for free Elc1 to 14 ns for the complex (Figure 5). From the distribution of T_1/T_2 ratios for the Elc1·peptide complex, the values for anisotropy A, effective correlation time $\tau_{c,eff}$, and rhombicity η were estimated based on the approach of Clore et al. (*52*) to be 1.87 ± 0.12, 15 ± 0.6 ns, and 0.95 ± 0.28, respectively (data not shown). The distribution of T_2 values was narrower than in the absence of peptide, and only few points fell slightly outside the contour for $S^2 = 1.0$. This indicates that the Elc1·peptide complex, in contrast to free Elc1, is not subject to strong chemical exchange phenomena. As in the absence of peptide, the data points corresponding to the flexible first half of loop 5 were located between the contours for $S^2 = 0.8$ and $S^2 = 0.6$, with T_2 values ranging from 0.1 to 0.17 s.

In summary, our data provide direct evidence that Elc1, upon binding of VHL peptide, undergoes conformational changes that result in a rigid, elongated overall structure, while maintaining intrinsic flexibility of loops 3 and, in particular, loop 5.

DISCUSSION

In this study, we provide conclusive evidence that Elc1 from *Saccharomyces cerevisiae* is a conformationally flexible monomer that undergoes extensive structural rearrangements upon binding to a model peptide derived from the VHL tumor suppressor protein.

One of the strengths of NMR spectroscopy is its virtually noninvasive nature, allowing us to study structural and dynamic properties of biomolecules in solution under close to physiological experimental conditions. Our NMR results on free and peptide-bound Elc1 provide additional information and reveal significant differences from the crystal structure of human ELC (*12*). First, peptide binding was shown to induce global conformational changes that result in a rigid, elongated overall shape not observed for free Elc1 (Figure 5). Whereas experimental restrictions (sample concentration, spectral overlap) as well as the complex T_1 vs T_2 patterns prevented us from performing a rigorous quantitative analysis of the relaxation data using the model-free formalism, comparison of the experimentally determined relaxation parameters with theoretically calculated values for the order parameter S^2 enabled us to detect anisotropic tumbling induced by peptide binding. Residues involved in the underlying conformational changes are spread throughout Elc1 rather than being confined to one particular region of the protein, in agreement with the widely distributed amide chemical shift changes reported (*23*). In particular, neither the relaxation nor the chemical shift data pinpoint residues within helix 4 itself as being primarily involved in the conformational changes. Second, helix 4 in free Elc1 was found to be in equilibrium with alternative conformations that can be shifted to a predominantly helical conformation by TFE or VHL peptide (Figure 4). This conclusion is supported by the chemical shift deviations and relaxation parameters for residues M86 and A93 in helix 4. These residues experience a very similar secondary structure environment in the absence and presence of TFE (see Supporting Information). However, their NMR relaxation behavior in the absence of TFE is more severely affected by chemical exchange mechanisms than the average of all residues, most likely due to conformational exchange. Third,

residues 69−77 in loop 5 are highly flexible even in the presence of VHL peptide (Figures 4 and 5). This is in contrast to ELC in the context of the crystal structure of the human VHL/ELC/ELB complex, where loop 5 was found to be well ordered (*12*). It remains to be established whether the exposed first part of loop 5 in human ELC is also well ordered in solution. Compared to human ELC, loop 5 of Elc1 has a three-residue insertion resulting in the sequence EDDDE (residues 72−76; Figure 1), which is likely to contribute to the flexibility of the loop. The insertion might be necessary to accommodate subtle differences between the structures of Elc1 and human ELC. Alternatively, it could provide a means of controlling the degrees of freedom for movements of helix 4 by an as yet unidentified effector. Interestingly, loop 5 bears even longer insertions in the homologous human and yeast Skp1 proteins (*12*).

A plot of T_1 versus T_2 values for free Elc1 revealed the existence of strong chemical exchange contributions to experimental T_2 values for a number of residues throughout the protein (Figure 5a). Principally, chemical exchange on a micro- to millisecond time scale could result from intramolecular conformational changes, intermolecular self-association, or a combination of both. The extent of chemical exchange contributions was significantly reduced in the presence of 10% TFE, and almost absent in the presence of peptide (Figure 5b,c), thus paralleling the conformational stabilization of helix 4. It can therefore be hypothesized that chemical exchange in free Elc1 is mainly a consequence of nonhelical conformations of helix 4. Loosely structured alternative conformations of the relatively hydrophobic helix 4, in combination with the extremely flexible, long loop 5, could participate in both intra- and intermolecular hydrophobic interactions with the folded core of Elc1. If those hydrophobic interactions are assumed to be predominantly unspecific in nature, then the relative proportion of intra- versus intermolecular interactions can be considered to be a function of protein concentration. Therefore, the chemical exchange processes detected in our relaxation measurements at protein concentrations below 400 μM, where NMR line widths were largely constant with protein concentration, could predominantly result from intramolecular conformational changes involving helix 4, whereas the excessive line broadening observed at millimolar concentrations could be caused by intermolecular self-association. Consistent with this possibility, we were unable to detect a significant nonmonomeric subpopulation of Elc1 in analytical ultracentrifuge experiments at concentrations below ca. 300 μM (Figure 2).

Recently, Botuyan and colleagues published a study reporting the effect of peptide binding on Elc1 structure (*23*). Our NMR results agree with respect to the conformational flexibility of helix 4 and the stabilizing effect of VHL peptide on Elc1 structure. However, whereas our data result from direct measurements of backbone dynamics, the assessment of structural stability by Botuyan et al. is solely based on a qualitative interpretation of line widths and peak intensities in ^{1}H,^{15}N-HSQC spectra. Their spectra were recorded at millimolar Elc1 concentrations that gave rise to excessive line broadening in their (*23*) and our (data not shown) measurements, i.e., under conditions of pronounced self-association. Based on our experiments performed at significantly lower Elc1 concentrations, we also came to different conclusions regarding the secondary structure content of free Elc1: we obtained clear evidence that helix 3 is fully formed (Figure 4, and Supporting Information). In addition, and consistent with the structure of human ELC, a turn between helices 1 and 2 was identified rather than one continuous helix.

The strongest discrepancy between the studies of Botuyan et al. and ourselves relates to the oligomeric state of Elc1. Based on sedimentation velocity and sedimentation equilibrium experiments, Botuyan et al. concluded that Elc1 forms a tetramer (*23*). They noted, however, that this conclusion is inconsistent with the sensitivity of their NMR experiments (*23*). On basis of the entire range of experimental data presented in our study, including analytical ultracentrifugation, analytical size exclusion chromatography, and NMR spectroscopy, we were unable to obtain any direct evidence for defined association states of Elc1 other than a monomer. One reason for this discrepancy could be that Botuyan et al. used a purification scheme that involved urea denaturation and subsequent refolding of Elc1 (*53*), whereas the Elc1 used in our study was purified as a native protein. It seems worth mentioning that in our hands the conformational changes of Elc1 upon peptide binding took place readily during the immediate acquisition of a ^{1}H,^{15}N-HSQC spectrum (ca. 30 min), rather than requiring several hours (*23*). This suggests that at the high Elc1 concentrations used by Botuyan et al., helix 4 might have been involved in unspecific aggregation of Elc1 that was disrupted by peptide.

The cellular concentration of Elc1 is unknown but can be assumed to be much less than 100 μM. Our rigorous analysis of Elc1 quaternary structure therefore suggests that the monomer is the physiologically relevant state of Elc1. The evolutionary conserved, conformationally flexible carboxy-terminal part of elongin C might be important to ensure binding to a variety of BC box proteins including VHL, thereby providing a further example of an induced folding mechanism in protein recognition (*48, 54*).

ACKNOWLEDGMENT

We thank Kam-Bo Wong for assistance with NMR experiments and data processing and for stimulating discussions; David Owen and Sebastien Poget for quantitative amino acid analyses and mass spectrometry, respectively; and Paul Barker for helpful comments on the manuscript.

SUPPORTING INFORMATION AVAILABLE

Two figures showing the results of analytical size exclusion chromatography and chemical shift analysis, respectively, and one table showing all experimental T_1 and T_2 values with standard errors (4 pages). This material is available free of charge via the Internet at http://pubs.acs.org.

REFERENCES

1. Hershko, A., and Ciechanover, A. (1992) *Annu. Rev. Biochem. 61*, 761−807.
2. Hochstrasser, M. (1996) *Annu. Rev. Genet. 30*, 405−439.
3. Hershko, A., and Ciechanover, A. (1998) *Annu. Rev. Biochem. 67*, 425−479.
4. Varshavsky, A. (1997) *Trends Biochem. Sci. 22*, 383−387.
5. Liakopoulos, D., Busgen, T., Brychzy, A., Jentsch, S., and Pause, A. (1999) *Proc. Natl. Acad. Sci. U.S.A. 96*, 5510−5515.

6. Lisztwan, J., Imbert, G., Wirbelauer, C., Gstaiger, M., and Krek, W. (1999) *Genes Dev. 13*, 1822−1833.
7. Iwai, K., Yamanaka, K., Kamura, T., Minato, N., Conaway, R. C., Conaway, J. W., Klausner, R. D., and Pause, A. (1999) *Proc. Natl. Acad. Sci. U.S.A. 96*, 12436−12441.
8. Pause, A., Lee, S., Worrell, R. A., Chen, D. Y., Burgess, W. H., Linehan, W. M., and Klausner, R. D. (1997) *Proc. Natl. Acad. Sci. U.S.A. 94*, 2156−2161.
9. Lonergan, K. M., Iliopoulos, O., Ohh, M., Kamura, T., Conaway, R. C., Conaway, J. W., and Kaelin, W. G., Jr. (1998) *Mol. Cell. Biol. 18*, 732−741.
10. Kamura, T., Koepp, D. M., Conrad, M. N., Skowyra, D., Moreland, R. J., Iliopoulos, O., Lane, W. S., Kaelin, W. G., Jr., Elledge, S. J., Conaway, R. C., Harper, J. W., and Conaway, J. W. (1999) *Science 284*, 657−661.
11. Kaelin, W. G., Jr., and Maher, E. R. (1998) *Trends Genet. 14*, 423−426.
12. Stebbins, C. E., Kaelin, W. G., Jr., and Pavletich, N. P. (1999) *Science 284*, 455−461.
13. Patton, E. E., Willems, A. R., and Tyers, M. (1998) *Trends Genet. 14*, 236−243.
14. Koepp, D. M., Harper, J. W., and Elledge, S. J. (1999) *Cell 97*, 431−434.
15. Tyers, M., and Rottapel, R. (1999) *Proc. Natl. Acad. Sci. U.S.A. 96*, 12230−12232.
16. Deshaies, R. J. (1999) *Annu. Rev. Cell. Dev. Biol. 15*, 435−467.
17. Skowyra, D., Koepp, D. M., Kamura, T., Conrad, M. N., Conaway, R. C., Conaway, J. W., Elledge, S. J., and Harper, J. W. (1999) *Science 284*, 662−665.
18. Bai, C., Sen, P., Hofmann, K., Ma, L., Goebl, M., Harper, J. W., and Elledge, S. J. (1996) *Cell 86*, 263−274.
19. Aso, T., Lane, W. S., Conaway, J. W., and Conaway, R. C. (1995) *Science 269*, 1439−1443.
20. Kamura, T., Sato, S., Haque, D., Liu, L., Kaelin, W. G., Jr., Conaway, R. C., and Conaway, J. W. (1998) *Genes Dev. 12*, 3872−3881.
21. Zhang, J. G., Farley, A., Nicholson, S. E., Willson, T. A., Zugaro, L. M., Simpson, R. J., Moritz, R. L., Cary, D., Richardson, R., Hausmann, G., Kile, B. J., Kent, S. B., Alexander, W. S., Metcalf, D., Hilton, D. J., Nicola, N. A., and Baca, M. (1999) *Proc. Natl. Acad. Sci. U.S.A. 96*, 2071−2076.
22. Aso, T., and Conrad, M. N. (1997) *Biochem. Biophys. Res. Commun. 241*, 334−340.
23. Botuyan, M. V., Koth, C. M., Mer, G., Chakrabartty, A., Conaway, J. W., Conaway, R. C., Edwards, A. M., Arrowsmith, C. H., and Chazin, W. J. (1999) *Proc. Natl. Acad. Sci. U.S.A. 96*, 9033−9038.
24. Miroux, B., and Walker, J. E. (1996) *J. Mol. Biol. 260*, 289−298.
25. Van Holde, K. E., and Baldwin, R. L. (1958) *J. Phys. Chem. 62*, 734−743.
26. Casassa, E. F., and Eisenberg, H. (1964) *Adv. Protein Chem. 19*, 287−395.
27. Kratky, O., Leopold, H., and Stabinger, H. (1973) *Methods Enzymol. 27*, 98−110.
28. Correia, J. J., Gilbert, S. P., Moyer, M. L., and Johnson, K. A. (1995) *Biochemistry 34*, 4898−4907.
29. Stafford, W. F., III (1992) *Anal. Biochem. 203*, 295−301.
30. Stafford, W. F., III (1994) *Methods Enzymol. 240*, 478−501.
31. Philo, J. S. (2000) *Anal. Biochem. 279*, 151−163.
32. Stafford, W. F., III (1997) *Curr. Opinion Biotechnol. 8*, 14−24.
33. Laue, T. M., Shah, B. D., Ridgeway, T. M., and Pelletier, S. L. (1992) in *Analytical Ultracentrifugation in Biochemistry and Polymer Science* (Harding, S. E., Rowe, A. J., and Horton, J. C., Eds.) pp 90−125, Royal Society of Chemistry, Cambridge.
34. Siegel, L. M., and Monty, K. J. (1966) *Biochim. Biophys. Acta 112*, 346−362.
35. le Maire, M., Rivas, E., and Moller, J. V. (1980) *Anal. Biochem. 106*, 12−21.
36. Piotto, M., Saudek, V., and Sklenar, V. (1992) *J. Biomol. NMR 2*, 661−665.
37. Grzesiek, S., and Bax, A. (1992) *J. Magn. Reson. 96*, 432−440.
38. Muhandiram, D. R., and Kay, L. E. (1994) *J. Magn. Reson. B 103*, 203-216.
39. Wittekind, M., and Mueller, L. (1993) *J. Magn. Reson. B 101*, 210−205.
40. Kraulis, P. J., Domaille, P. J., Campbell-Burk, S. L., Van Aken, T., and Laue, E. D. (1994) *Biochemistry 33*, 3515−3531.
41. Wagner, G. (1993) *Curr. Opin. Struct. Biol. 3*, 748−754.
42. Derome, A. E. (1987) *Modern NMR Techniques for Chemistry Research*, Pergamon Press, Oxford.
43. Ng, R. W. M., Arooz, T. A., Yam, C. H., Chan, I. W. Y., Lau, A. W. S., and Poon, R. Y. C. (1998) *FEBS Lett. 438*, 183−189.
44. Goodman, M., Listowsky, I., and Masuda, Y. F. B. (1963) *Biopolymers 1*, 33−42.
45. Nelson, J. W., and Kallenbach, N. R. (1986) *Proteins: Struct., Funct., Genet. 1*, 211−217.
46. Jasanoff, A., and Fersht, A. R. (1994) *Biochemistry 33*, 2129−2135.
47. Waterhous, D. V., and Johnson, W. C. J. (1994) *Biochemistry 33*, 2121−2128.
48. Kim, A. S., Kakalis, L. T., Abdul-Manan, N., Liu, G. A., and Rosen, M. K. (2000) *Nature 404*, 151−158.
49. Kay, L. E., Torchia, D. A., and Bax, A. (1989) *Biochemistry 28*, 8972−8979.
50. Lipari, G., and Szabo, A. (1982) *J. Am. Chem. Soc. 104*, 4546−4559.
51. Aso, T., Haque, D., Barstead, R. J., Conaway, R. C., and Conaway, J. W. (1996) *EMBO J. 15*, 5557−5566.
52. Clore, G. M., Gronenborn, A. M., Szabo, A., and Tjandra, N. (1998) *J. Am. Chem. Soc. 120*, 4889−4890.
53. Koth, C. M., Botuyan, M. V., Moreland, R. J., Jansma, D. B., Conaway, J. W., Conaway, R. C., Chazin, W. J., Friesen, J. D., Arrowsmith, C. H., and Edwards, A. M. (2000) *J. Biol. Chem. 275*, 11174−11180.
54. Wright, P. E., and Dyson, H. J. (1999) *J. Mol. Biol. 293*, 321−331.

BI0008231